Physica B: Condensed Matter 564 (2019) 179–185

Contents lists available at ScienceDirect

Physica B: Condensed Matter

journal homepage: www.elsevier.com/locate/physb

Facile sono-chemical synthesis of nanocrystalline MnO_2 for catalytic and capacitive applications

Kajal Rajrana, Aayush Gupta, Rameez Ahmad Mir, O.P. Pandey*

Functional Materials Lab, School of Physics and Materials Science, Thapar Institute of Engineering and Technology, Patiala, 147004, India

ARTICLE INFO

Keywords:
MnO_2
Adsorption
Photodegradation
HER
EDLC

ABSTRACT

In this reported work, the potential application of MnO_2 nanopowder for photocatalytic and the electrocatalytic applications is explored. The MnO_2 nanopowder has been synthesized through sonochemical route using $KMnO_4$ and poly-ethylene glycol as the reducing agent. Structural and optical analysis (XRD, TEM, FTIR, XPS and UV–visible) confirmed the formation of nanocrystalline MnO_2 network. The adsorption and photocatalytic performance of synthesized MnO_2 was tested for degradation of methylene blue dye and p-nitrophenol (2 mg/L) under dark chamber and household CFL lamp exposure, respectively. The electrochemical studies in alkaline (0.5 M KOH) medium shows the electric double layer capacitance of 7.4 $mFcm^{-2}$ suggesting its potential application for energy storage devices. The synthesized compound exhibited excellent stability after 1000 CV cycles (~4% current loss) where Volmer reaction was observed as the rate determining step for the electrocatalytic hydrogen evolution reaction.

1. Introduction

The requirement of fresh and clean water is increasing continuously to cater the needs of society. At the same time, population pressure has led to development of many new industries. Among these industries like textile, pulp and paper, food leather, printing, etc. consume lot of fresh water and dispose of contaminated water into soil. In this process, every year about 800,000 tons of synthetic dyes (non-biodegradable, mutagenic and carcinogenic) are dumped into natural water resources causing severe damage to aquatic flora-fauna by depleting the dissolved oxygen in water. There are various physical, chemical and biological techniques to extract or degrade such organic effluents [1–6]. Among these, advanced oxidation process (AOP) is the most efficient degradation of organic pollutants and pesticides than other conventional techniques. The semiconductor photocatalysis is considered as a green approach and efficient process [7,8]. Due to photons-catalyst interaction, initially generated electron-hole pair participates in various photochemical reactions and generates highly reactive radicals ($\cdot OH^-$ and $\cdot O_2^-$) which further oxidize the pollutants to form mineral acids, CO_2 and H_2O [9,10].

Conventionally, semi-conducting and metallic compounds such as TiO_2, ZnO, CdS, ZnS, CeO_2 and ZrC are used for the same purpose as photocatalysts [11–16]. In recent years, a plateau has occurred in the field of applicability of ZnO and TiO_2 as photocatalyst and their excitation under UV-region (3% of solar spectrum) limits their usability. However, their applicability has been enhanced by tailoring the optical band gap of the photocatalyst by doping or forming a heterostructure, but their performance has some limitations [17–19]. Among all, MnO_2 exhibits non-toxicity, excellent ambient chemical and physical properties due to their polymorphic nature [17,20–25]. Conventionally, it is being used as cathode material as electrochemical capacitor in fuel cells due to its large initial capacity [17,24,26,27]. Its heterostructure with a variety of compounds such as CNTs [28], graphene [29], polyaniline [30], Ag/rGO [31] enhanced the charge storage capacity of MnO_2 due to better transfer of electrons [32].

Further, excitation in the visible light region and n-type semiconducting properties induce its applicability as a photocatalyst [27,33]. In MnO_2, it is attributed that d-d electronic transitions are known to occur because of partially filled d-orbitals during irradiation thus, it can work as an effective photocatalyst without any doping [34]. High specific surface area and sufficiently active sites of MnO_2 are the most important parameters for adsorption process [35]. With these properties, considerable redox activity of MnO_2 makes it suitable for photocatalytic degradation. In literature, various studies have shown the adsorption and catalytic ability of MnO_2 alone as well as support of the other compounds to enhance their performance. Gheju et al. [36] and Wakeel et al. [37] proposed the use of MnO_2 for the removal of Cr^{4+} and Pb^{2+} from contaminated water through adsorption. Some

* Corresponding author.
E-mail address: oppandey@thapar.edu (O.P. Pandey).

https://doi.org/10.1016/j.physb.2019.04.002
Received 22 February 2019; Received in revised form 30 March 2019; Accepted 1 April 2019
Available online 02 April 2019
0921-4526/

research groups have also studied the photocatalytic behavior of MnO_2 and its heterostructure for the removal of different organic effluents without sufficient kinetic analysis and responsible mechanism [38–40]. Being highly efficient photocatalyst, the electrocatalytic application of MnO_2 for water splitting through HER for the production of renewable and green energy fuel widens its research area. MnO_2 has been studied for its capacitive behavior with its variety of morphologies and combinations with other compounds, its applicability as photocatalyst and catalytic kinetics is yet to be explored.

Considering these aspects, in this wok we report a facile route to synthesize nano-crystalline MnO_2 through single step sonochemical route to understand its adsorption, photo- and electro- catalytic kinetics. The novelty of this work is the synthesis route followed here. The ultrasonication process provide additional- vibrational energy to enhance the rate of chemical reaction which facilitate the rapid nucleation of fine particles. Moreover, ultrasonic irradiation enhances the reduction of $KMnO_4$ yielding MnO_2 through the pyrolysis of poly ethylene glycol (PEG) [41]. The capacitive behavior of synthesized MnO_2 has also been studied to understand the effect of structured network on the charge storage capacity.

2. Experimental

2.1. Synthesis of MnO_2 and characterization

MnO_2 nanopowder were prepared by the reduction of $KMnO_4$ (SD-fine chem Ltd) with polyethylene glycol (PEG) (Lab. Reagents & Fine Chemicals) through ultrasonication. Typically, 0.5 g of $KMnO_4$ was dissolved in 60 ml of distilled water (DW) followed by the addition of 5.5 g PEG in the solution with continuous stirring for 10–15 min at 60 °C. Thereafter, brown colored precipitates were obtained by sonication (LABMAN Scientific Instruments; 50 W; 220 V; 40 kHz) after 30 min. Then the solution was filtered and washed several times with DW and ethanol alternatively and dried in a vacuum oven at 70 °C for 12 h.

The crystallographic information was obtained by X-ray diffraction (XRD) technique using Cu (K_α = 1.54 Å) radiations in the range of 20–80° (2θ) with 0.0120° step size on *PANalytical Xpert-Pro* diffractometer. Transmission electron microscopy (TEM) was performed on *JEOL 2100F* (200 kV) to understand the morphology of the prepared sample. The absorption spectra and emission spectra of the prepared sample were recorded by using Double beam UV–Visible spectrophotometer (*Hitachi U-3900H*) and Photoluminescence (PL) spectrometer (*G9800A*). Further, structural and chemical composition of the prepared sample were observed with the help of FTIR and X-ray photo spectroscopy (XPS). The presence of various functional groups and vibrational modes were observed using FTIR (*Perkin Elmer-Spectrum-RF-1*) in the range 400–2000 cm^{-1} at room temperature. XPS data was obtained on *PHI 5000 Versa Prob II, FEI Inc.* with the help of Al Kα radiation (1486.7 eV, C1s; 284.4 eV as calibration binding energy).

2.2. Adsorption and photocatalytic test

To understand the adsorption and photocatalytic performance of the prepared MnO_2 sample, methylene blue (MB) dye and N-phenol were taken as model organic compounds. For both the studies, 100 ml of 2.0 mg/L solution of both compounds was prepared and 10 mg of prepared MnO_2 catalyst was added to it. The prepared mixture was kept in the dark chamber for 30 min. An aliquot of 3 ml was extracted at an interval of 2 min and measure the absorption at 664 and 400 nm (characteristic absorption wavelength of MB dye and N-phenol, respectively) to calculate the amount of adsorbed dye on the surface of prepared catalyst. Thereafter, the solution was exposed to visible irradiation under household CFL lamp (85 W; 8900 lx) for 120 min in which sampling was carried out at an interval of 30 min and measured the absorption at same wavelengths. Further, kinetic studies for the photochemical reactions has been carried out based on our previous report [12].

2.3. Electrocatalytic test

The electrochemical activity of the as-prepared samples was investigated by *Bio-logic EC Lab SP300* standard setup. In the three-electrode system platinum was used as the counter electrode, saturated calomel electrode (SCE) as the reference electrode and the working electrode was prepared manually. For fabrication of the working electrode, 1 mg of the sample was dispersed in 250 µL of ethanol and the solution was sonicated for 25 min to achieve uniform dispersion of particles. The top surface of glassy carbon electrode (GCE) having a surface area of 0.070 cm^2 was drop-casted by10 µL of the above dispersed solution. A single drop of Nafion 117 solution (Sigma Aldrich) from 10 µL was put onto the GCE top and was dried overnight.

The three-electrodes were dipped in the working cell filled with basic electrolyte 0.5 M KOH. All the measurements were done for the reversible hydrogen electrode (RHE). The SCE measurements were converted to RHE by using eq. (1) [42]

$$\boldsymbol{RHE} = \boldsymbol{V_{SCE}} + 0.059 \times \boldsymbol{pH} + 0.243 \quad (1)$$

where V_{SCE} is the voltage with respect to SCE.

3. Results and discussion

3.1. XRD, UV–visible spectroscopy, FTIR and TEM microscopy

Fig. 1a represents the XRD pattern of synthesized MnO_2 sample, which exhibit nano-scale crystallites corresponding to broad peaks at 37° and 66° as reported by different research groups [26,27,41,43,44]. The formation of MnO_2 has also been observed with optical absorbance spectroscopy in which the calculated optical band gap was calculated to be 2.53 eV as shown in the inset of Fig. 1b [16]. Further, FTIR spectra (Fig. 1c) of as-synthesized MnO_2 sample confirmed the formation of MnO_2 where the broad transmittance bands were observed at 500–650, 1000–1100, 1346 and 1413 cm^{-1} are corresponding to the O−Mn−O, Mn−O (MnO_6 octahedra), Mn−OH, Mn=O and bending of Mn−OH, respectively [45–48]. Further, broad transmittance band around ~1585 cm^{-1} is associated to the weak stretching of OH bond [45]. Moreover, TEM micrographs have also supported the XRD results, which show a very large network like morphology of prepared sample as shown in Fig. 2. It suggests that the open porous network like

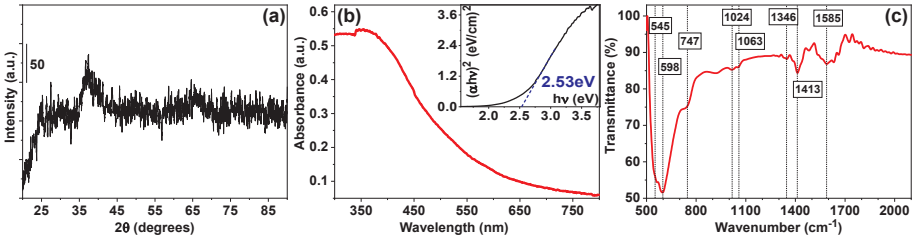

Fig. 1. (a) XRD, (b) optical absorption spectra (inset) and (c) FTIR spectra of nanocrystalline MnO_2.

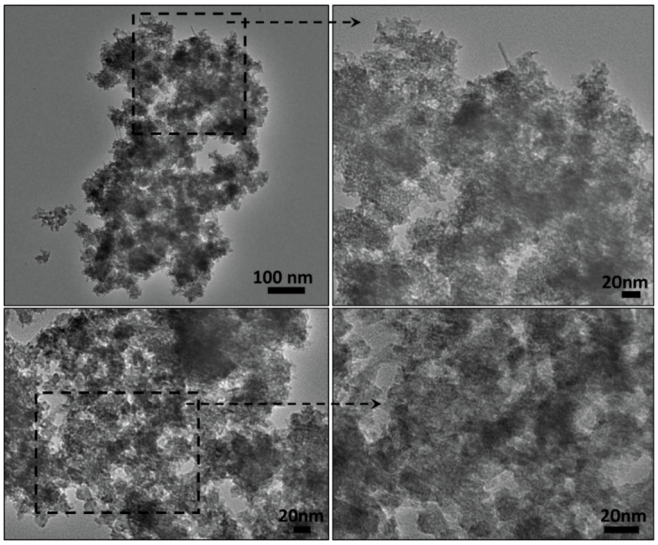

Fig. 2. TEM micrographs of MnO_2 nanopowder suggesting the open porous network.

structure consisting of very small crystallites as shown in Fig. 3 [27]. Further, SAED pattern exhibited diffused ring like pattern which is in tune to the peak observed at ~37° in XRD pattern [41]. HR-TEM images at different regions with lattice fringing have confirmed the formation of nanocrystalline MnO_2 as shown in Fig. 3a–f.

3.2. XPS spectroscopy

In order to estimates the chemical composition of synthesized MnO_2 samples on the surface, X-ray photoelectron spectroscopy (XPS) analysis was done. Fig. 4a confirmed the presence of Mn (2p, 3s and 3p) and O (1s) on the surface of the catalyst while, presence of carbon (1s) can be associated to the calibration element or adhesive tape. HR-XPS spectra of Mn2p (Fig. 4b) revealed the presence of multiple oxidation states of Mn in the form of Mn^{2+}, Mn^{3+} and Mn^{4+} associated to 641.1, 642.2 and 644.3 eV respectively [49,50]. The volume fraction of all these three oxidation states follows 33.65, 44.13 and 22.22%, respectively. Moreover, HR-XPS spectra of O1s (Fig. 4c) suggested the presence of lattice oxygen (529.3 eV; 28.18%) along with surface oxygen species (O_2^-, O^- *and* O_2^{2-}; 531.9 eV; 29.17%) and adsorbed water (532.5 eV; 42.64%) [50]. The higher volume fraction of adsorbed species than lattice oxygen may be associated to the porous network like morphology of the synthesized catalyst. Further, the valence band spectrum of the catalyst suggested the potential of the highest level of valence band (VBE), as −0.17 eV as shown in Fig. 4d. Hence, the position of power level of conduction band (CBE) can be calculated as 2.36 eV ($CBE = E_g + VBE$). The presence of various surface functional groups is responsible for the catalytic reactions that is discussed in subsequent sections 3.3 and 3.4.

3.3. Adsorption and photodegradation study

For the adsorption and photocatalytic study of synthesized MnO_2 nanopowder, two different organic effluents have been used (MB dye and N-phenol) which have excitation in visible and UV region (respectively) to eliminate the effect of dye sensitization. Prior to irradiation, photocatalyst was dispersed in the both solutions for 30 min and the decrease in the concentration of solution obtained during the establishment of adsorption-desorption equilibrium is shown in Fig. 5a. Fig. 5a suggest the saturation of adsorption of molecules (MB and N-phenol) on the surface of catalyst and Fig. 5b and c represent the pseudo first and second order reaction kinetics for MB dye and N-phenol. Based on the quality of fitting (R^2), it has been observed that the adsorption of MB dye and N-phenol followed pseudo second order kinetics i.e. chemisorption at the rate of 0.0432 and 0.4792 min^{-1} (respectively) as shown in Fig. 5c. The observed relationship might be asserted to the attachment of oxygen species (O_2^-, O^- *and* O_2^{2-}) to the effluent molecule as observed in XPS spectra (Fig. 4c).

As a result of adsorption study, 96.2% and 86.9% adsorption of MB dye and N-phenol (respectively) has been observed on the surface of synthesized MnO_2 nanopowder. Thereafter, solutions were irradiated under CFL lamp and variation in their concentration was measured and significant degradation (49%; MB dye and 42%; N-phenol) was observed in 120 min as shown in Fig. 6a. The observed discoloration trend confirmed the photodegradation of both the organic effluents under visible radiations rather dye sensitization [51]. Further, the rate kinetics suggested the simultaneous action of pseudo first and second order law during the photodegradation of MB dye and N-phenol as shown in Fig. 6b and c, respectively [12].

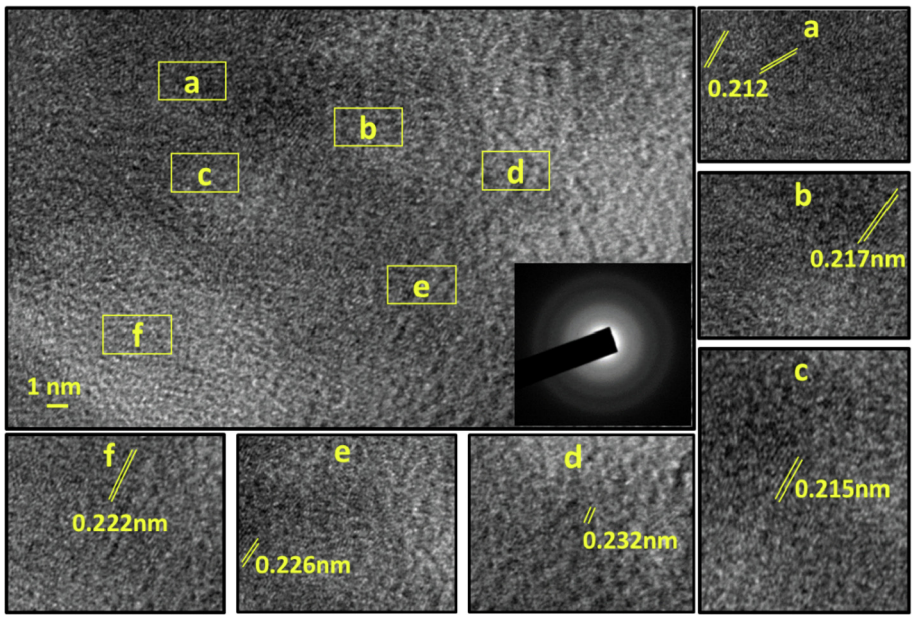

Fig. 3. HR-TEM micrograph of MnO_2 nanopowder suggesting the presence of nano-crystallites embedded in an amorphous network (SAED pattern).

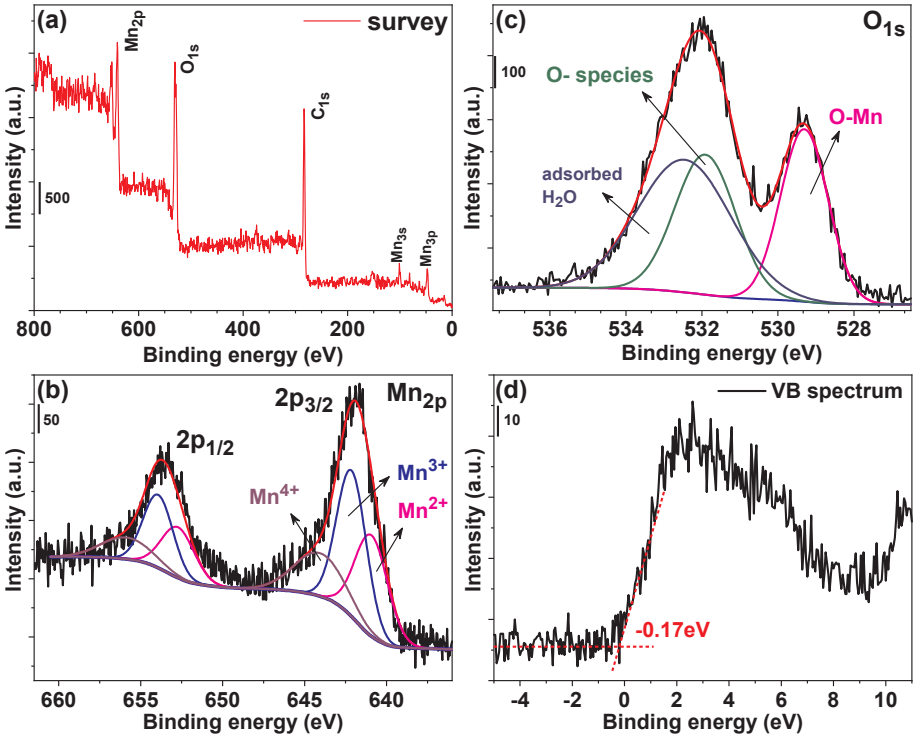

Fig. 4. XPS spectra of prepared MnO_2 sample. Survey spectrum (a); HR-XPS spectra of Mn_{2p} (b), O_{1s} (c) and valence band spectra (d).

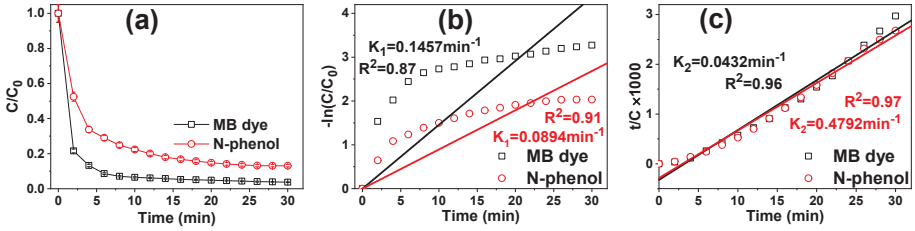

Fig. 5. Adsorption kinetics of MB dye and N-phenol (a) C/C_0 vs. time; (b) pseudo first order and (c) pseudo second order reaction kinetics.

Fig. 7 represents the schematic mechanism responsible for the photodegradation of both organic compounds. Photo excited electrons-holes participate in the formation of superoxide onion radical ($\cdot O_2^-$) and hydroxyl radical ($\cdot OH$) at conduction and valance band, respectively as mentioned below:

$$MnO_2 + photon \rightarrow MnO_2 + h^+ + e^- \quad (2)$$

$$OH^- + h^+ \rightarrow \cdot OH \quad (3)$$

$$O_2 + e^- \rightarrow O_2^- \quad (4)$$

$$O_2^- + H_2O \rightarrow \cdot OH + OH^- \quad (5)$$

$$MnO_2 + MB^* \rightarrow MB^{\cdot +} + MnO_2^- \quad (6)$$

$$MnO_2^- + O_2 \rightarrow MnO_2 + O_2^- \quad (7)$$

$$MnO_2^- + O_2^- + h^+ \rightarrow MnO_2 + HO_2^- \quad (8)$$

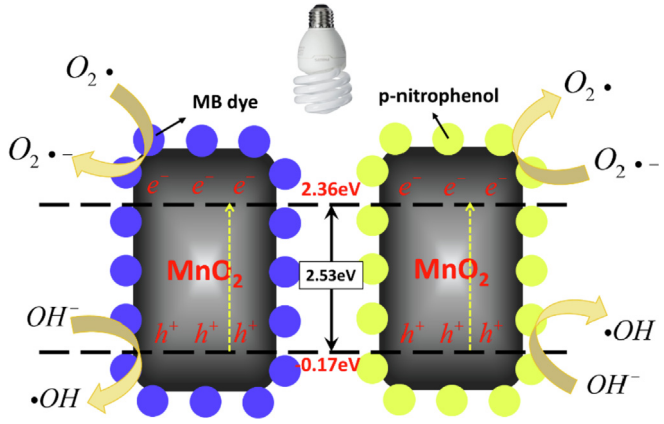

Fig. 7. Schematic representation of photodegradation mechanism with MnO_2.

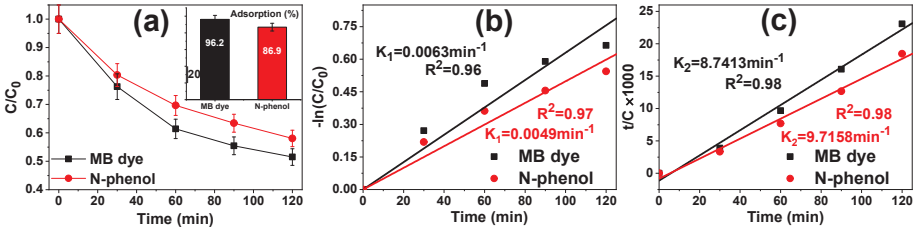

Fig. 6. Photodegradation kinetics of MB dye and N-phenol (a) C/C_0 vs. time with adsorption of adsorbate on the synthesized catalyst (inset); (b) pseudo first order and (c) pseudo second order reaction kinetics.

$$HO_2^- + h^+ \rightarrow H_2O_2 \quad (9)$$

$$H_2O_2 + e^- \rightarrow \cdot OH + OH^- \quad (10)$$

$$Mn^{4+} \overset{e^-}{\leftrightarrow} Mn^{3+} \overset{e^-}{\leftrightarrow} Mn^{2+} \quad (11)$$

$$Mn^{2+} \overset{h^+}{\leftrightarrow} Mn^{3+} \overset{h^+}{\leftrightarrow} Mn^{4+} \quad (12)$$

Direct photoexcitation of MnO_2 exhibited the degradation of both compounds following equations (2)–(5) through the transfer of charge carriers from catalyst to dye molecules resulting the formation of different radicals. While, in the case of MB dye, indirect excitation of the catalyst is also possible, which can be expressed with the help of equation (6)–(10), resulting in the photo-oxidation of MB dye [52]. Moreover, the presence of multiple oxidation states of Mn (as observed in XPS results) would further promote the photochemical reaction as charge trap center by delaying the recombination [15]. Thereafter, these reactive radicals would decompose the absorbed molecules during the visible exposure resulting either lighter non-toxic organic molecules or $CO_2 + H_2O$.

3.4. Electrocatalytic study

The capacitive performance of MnO_2 nanostructures is evaluated by CV analysis. Fig. 8a shows the CV curves of MnO_2 nanostructures at multiple scan rate of 20–200 $mVsec^{-1}$. The rectangular loop in the potential window (0.77–0.97 V) along the current-potential axis without any redox peak, indicates the non-faradic capacitive behavior synthesized nano structures [53]. The calculated electric double layer capacitance (EDLC, C_{dl}; Fig. 8b) and specific capacitance (SC) is 7.9 $mFcm^{-2}$ and 13.8 Fg^{-1}, respectively. The C_{dl} value exhibited the large electrochemically active surface area of these synthesized MnO_2 nanostructures and revealed the enhanced capacitance in basic electrolyte. The enhancement in the charge storage capacity is mainly due to the smaller crystallite size as determined from TEM. The porous network exhibited by TEM also improves the charge kinetic rate on the surface [44]. The higher C_{dl} and SC of the synthesized MnO_2 nanostructures shows the enhancement in charge storage capacity with respect to the reported and developed capacitor materials [42,54,55]. Furthermore, MnO_2 nanostructures have excellent long duration cycle stability for 2000 CV cycles as shown in Fig. 8c. The only distortion observed is with respect to first CV cycle, which remains constant thereafter for all the corresponding cycles. The specific capacitance retention (%) with respect to CV cycle number is shown in Fig. 8d. The curve reveals the only loss of retention by 13% for 2000 cycles, which is higher than the other synthesized capacitance electrode materials [29,41,42,54,56,57]. The higher stability of the synthesized MnO_2 structure might correspond to its poor crystallinity and unique morphological characteristics which inhibit the poisoning of cathode during charging and discharging. The EDLC utilizes surface characteristics for reversible ion adsorption at the surface or inside pores to improve the capacitance performance as well as retention to store charge. The mechanism of energy storage by MnO_2 materials having nearly amorphous nature and showing non redox reversible redox CV curves is generally based on surface adsorption/desorption of H^+ at the surface [55,56,58]. This phenomenon is responsible for the EDLC behavior of synthesized nanostructures, which is in agreement with the CV curve as also predicted by Lukatskaya et al. [59]. The lattice defects introduced during the synthesis due to lattice defects or oxygen vacancies improve the charge storage performance [60]. The results reveal the potential application of synthesized MnO_2 phase for double layer capacitor applications.

To understand the adsorption/desorption kinetics of the synthesized material and its potential use as electrocatalyst for water splitting through hydrogen evolution reaction (HER), the linear sweep voltammetry (LSV) and Tafel analysis studies were done as shown in Fig. 8e and f, respectively. The Tafel slope of 120.7 $mVdec^{-1}$ determines the Volmer reaction as the rate determining step for HER [42,53,54]. Volmer reaction studies also predict the lower adsorption/desorption kinetics of the synthesized MnO_2 due to low crystallinity and uneven wide pore size distribution in porous network. The same mechanism is also responsible for charge storage in low crystalline MnO_2 based capacitors. The surface characteristics need to be modified to enhance the charge transfer kinetics for enhancement in HER and storage ability. The current density value of 30 $mAcm^{-2}$ initially show the higher electron transfer rate of MnO_2 nanostructures. The lower crystallite size and open porous network like morphology enhances the charge transfer rate and improves the current density value in the given voltage. The continuous network like morphology exhibited by synthesized MnO_2 provides more active sites available for the electrocatalytic activity and enhance current density. The stability is an important parameter for the commercial application of the synthesized material for HER. The stability was tested via CV analysis performed in voltage window −0.2 to −0.9 V at a scan rate of 100 $mVsec^{-1}$ for 1000 cycles. The LSV plot performed after 1000 CV cycles shows the loss of current density by ~4% as shown in Fig. 8e. The results predict the synthesized material as potential electrocatalyst for HER in basic electrolyte with higher stability. The stability can be enhanced by changing the oxygen species present on the surface to improve the corrosion resistance of synthesized MnO_2 in basic electrolyte. The higher content of O-species (observed in XPS results) on the surface exhibited the enhanced corrosion resistance and stability. The results reveal the use of synthesized material for charge storage devices and also as the stable electrocatalyst for green/hydrogen energy production.

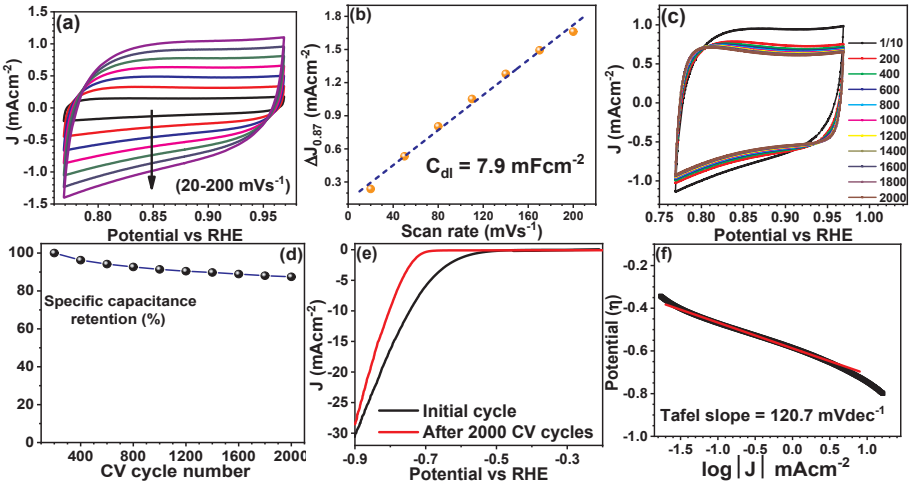

Fig. 8. (a) cyclic voltammetry (CV) curve with variable scan rate; (b) electric double layer capacitance (EDLC); (c) CV plots representing the stability upto 2000 cycles in basic medium; (d) specific capacitance retention vs. number of cycles; (e) linear sweep voltammetry (LSV) in basic medium (0.5 M KOH) and (f) Tarek slope in basic medium for the synthesized MnO_2 nanopowder.

4. Conclusion

MnO_2 nanopowder has been synthesized through a facile single step sonochemical route through the reduction of $KMnO_4$ with PEG. XRD, UV–visible spectroscopy and TEM results confirmed the formation of nanocrystalline network of MnO_2 with ultra-small crystallites (~2–3 nm) having 2.53 eV optical band gap. FTIR spectroscopy suggested the presence of MnO_6 octahedra as basic constituent with different vibrating Mn−O functional groups and XPS confirmed the presence of Mn in multiple oxidation states (2+, 3 + and 4+). Further, adsorption study revealed the adsorption of MB dye and p-nitrophenol has been saturated in 30min with 96 and 86% efficiency (respectively) following chemisorption kinetics. Further, photodegradation of both the molecules under household CFL lamp has been observed with ~50 and ~42% efficiency through the simultaneous physi- and chemisorption kinetics. Electrocatalytic results confirmed the excellent stability of synthesized MnO_2 up to 2000 cycles in alkaline medium (0.5 M KOH) with Volmer reaction as the rate determining step. The potential application of MnO_2 as capacitor with durability and excellent stability for HER widens the research area for the electrocatalytic water splitting.

References

[1] H. Huang, J. Liu, P. Zhang, D. Zhang, F. Gao, Investigation on the simultaneous removal of fluoride, ammonia nitrogen and phosphate from semiconductor wastewater using chemical precipitation, Chem. Eng. J. 307 (2017) 696–706, https://doi.org/10.1016/j.cej.2016.08.134.

[2] V. Colla, T.A. Branca, F. Rosito, C. Lucca, B.P. Vivas, V.M. Delmiro, Sustainable Reverse Osmosis application for wastewater treatment in the steel industry, J. Clean. Prod. 130 (2016) 103–115, https://doi.org/10.1016/j.jclepro.2015.09.025.

[3] C.Y. Teh, P.M. Budiman, K.P.Y. Shak, T.Y. Wu, Recent advancement of coagulation-flocculation and its application in wastewater treatment, Ind. Eng. Chem. Res. 55 (2016) 4363–4389, https://doi.org/10.1021/acs.iecr.5b04703.

[4] S. De Gisi, G. Lofrano, M. Grassi, M. Notarnicola, Characteristics and adsorption capacities of low-cost sorbents for wastewater treatment: a review, Sustain. Mater. Technol. 9 (2016) 10–40, https://doi.org/10.1016/j.susmat.2016.06.002.

[5] M. Mehrjouei, S. Müller, D. Möller, A review on photocatalytic ozonation used for the treatment of water and wastewater, Chem. Eng. J. 263 (2015) 209–219, https://doi.org/10.1016/j.cej.2014.10.112.

[6] Y. Feng, L. Yang, J. Liu, B.E. Logan, Electrochemical technologies for wastewater treatment and resource reclamation, Environ. Sci. Water Res. Technol. 2 (2016) 800–831, https://doi.org/10.1039/c5ew00289c.

[7] S. Dong, J. Feng, M. Fan, Y. Pi, L. Hu, X. Han, M. Liu, J. Sun, J. Sun, Recent developments in heterogeneous photocatalytic water treatment using visible light-responsive photocatalysts: a review, RSC Adv. 5 (2015) 14610–14630, https://doi.org/10.1039/c4ra13734e.

[8] P.A.K. Reddy, P.V.L. Reddy, E. Kwon, K.H. Kim, T. Akter, S. Kalagara, Recent advances in photocatalytic treatment of pollutants in aqueous media, Environ. Int. 91 (2016) 94–103, https://doi.org/10.1016/j.envint.2016.02.012.

[9] J. Xiao, Y. Xie, H. Cao, Organic pollutants removal in wastewater by heterogeneous photocatalytic ozonation, Chemosphere 121 (2015) 1–17, https://doi.org/10.1016/j.chemosphere.2014.10.072.

[10] S. Teixeira, R. Gurke, H. Eckert, K. Kühn, J. Fauler, G. Cuniberti, Photocatalytic degradation of pharmaceuticals present in conventional treated wastewater by nanoparticle suspensions, J. Environ. Chem. Eng. 4 (2016) 287–292, https://doi.org/10.1016/j.jece.2015.10.045.

[11] P. Singla, M. Sharma, O.P. Pandey, K. Singh, Photocatalytic degradation of azo dyes using Zn-doped and undoped TiO2 nanoparticles, Appl. Phys. A. 116 (2014) 371–378, https://doi.org/10.1007/s00339-013-8135-z.

[12] M. Mittal, M. Sharma, O.P. Pandey, UV – visible light induced photocatalytic studies of Cu doped ZnO nanoparticles prepared by co-precipitation method, Sol. Energy 110 (2014) 386–397, https://doi.org/10.1016/j.solener.2014.09.026.

[13] M. Kaur, O.P. Pandey, M. Sharma, Synthesis and characterization of Mn doped ZnCdS core shell nanostructures QDs using a chemical precipitation route, AIP Conf. Proc. 1724 (2016), https://doi.org/10.1063/1.4945177.

[14] J. Kaur, A. Gupta, O.P. Pandey, Photocatalytic study of ZnS-Ag2S nanocomposites-effect of thioglycerol, Sol. Energy 176 (2018) 678–687, https://doi.org/10.1016/j.solener.2018.10.077.

[15] M. Mittal, A. Gupta, O.P. Pandey, Role of oxygen vacancies in Ag/Au doped CeO2 nanoparticles for fast photocatalysis, Sol. Energy 165 (2018) 206–216, https://doi.org/10.1016/j.solener.2018.03.033.

[16] A. Singh Vig, A. Gupta, O.P. Pandey, Efficient photodegradation of methylene blue (MB) under solar radiation by ZrC nanoparticles, Adv. Powder Technol. 29 (2018) 2231–2242, https://doi.org/10.1016/j.apt.2018.06.007.

[17] J.G. Wang, F. Kang, B. Wei, Engineering of MnO2-based nanocomposites for high-performance supercapacitors, Prog. Mater. Sci. 74 (2015) 51–124, https://doi.org/10.1016/j.pmatsci.2015.04.003.

[18] M.A. Barakat, M.H. Ramadan, M.A. Alghamdi, S.S. Algarny, H.L. Woodcock, J.N. Kuhn, Remediation of Cu(II), Ni(II), and Cr(III) ions from simulated wastewater by dendrimer/titania composites, J. Environ. Manag. 117 (2013) 50–57, https://doi.org/10.1016/j.jenvman.2012.12.025.

[19] K.M. Lee, C.W. Lai, K.S. Ngai, J.C. Juan, Recent developments of zinc oxide based photocatalyst in water treatment technology: a review, Water Res. 88 (2016) 428–448, https://doi.org/10.1016/j.watres.2015.09.045.

[20] Z. Dai, X. Yu, C. Huang, M. Li, J. Su, Y. Guo, H. Xu, Q. Ke, Nanocrystalline MnO2 on an activated carbon fiber for catalytic formaldehyde removal, RSC Adv. 6 (2016) 97022–97029, https://doi.org/10.1039/c6ra15463h.

[21] S. Guan, W. Li, J. Ma, Y. Lei, Y. Zhu, Q. Huang, X. Dou, A review of the preparation and applications of MnO2 composites in formaldehyde oxidation, J. Ind. Eng. Chem. 66 (2018) 126–140, https://doi.org/10.1016/j.jiec.2018.05.023.

[22] S. Das, A. Samanta, S. Jana, Light-Assisted synthesis of hierarchical flower-like MnO2Nanocomposites with solar light induced enhanced photocatalytic activity, ACS Sustain. Chem. Eng. 5 (2017) 9086–9094, https://doi.org/10.1021/acssuschemeng.7b02003.

[23] I. Khan, M. Sadiq, I. Khan, K. Saeed, Manganese Dioxide Nanoparticles/Activated Carbon Composite as Efficient UV Manganese Dioxide Nanoparticles/Activated Carbon Composite as Efficient UV and Visible-Light Photocatalyst, (2019), https://doi.org/10.1007/s11356-018-4055-y.

[24] J. Zhao, Z. Tao, J. Liang, J. Chen, Facile synthesis of nanoporous γ-MnO2 structures and their application in rechargeable Li-ion batteries, Cryst. Growth Des. 8 (2008) 2799–2805, https://doi.org/10.1021/cg701044b.

[25] M. Xu, L. Kong, W. Zhou, H. Li, Hydrothermal synthesis and pseudocapacitance properties of α-MnO 2 hollow spheres and hollow urchins, J. Phys. Chem. C 111 (2007) 19141–19147, https://doi.org/10.1021/jp076730b.

[26] Q. Liu, S. Ji, J. Yang, H. Wang, B.G. Pollet, R. Wang, Enhanced cycleability of amorphous MnO2 by covering on α-MnO2 needles in an electrochemical capacitor, Materials (Basel) 10 (2017) 1–10, https://doi.org/10.3390/ma10090988.

[27] H.Q. Wang, G.F. Yang, Q.Y. Li, X.X. Zhong, F.P. Wang, Z.S. Li, Y.H. Li, Porous nano-MnO2: large scale synthesis via a facile quick-redox procedure and application in a supercapacitor, New J. Chem. 35 (2011) 469–475, https://doi.org/10.1039/c0nj00712a.

[28] L. Li, Z.A. Hu, N. An, Y.Y. Yang, Z.M. Li, H.Y. Wu, Facile synthesis of MnO2/CNTs composite for supercapacitor electrodes with long cycle stability, J. Phys. Chem. C 118 (2014) 22865–22872, https://doi.org/10.1021/jp505744p.

[29] Y. Xiong, M. Zhou, H. Chen, L. Feng, Z. Wang, X. Yan, S. Guan, Synthesis of honeycomb MnO2 nanospheres/carbon nanoparticles/graphene composites as electrode materials for supercapacitors, Appl. Surf. Sci. 357 (2015) 1024–1030, https://doi.org/10.1016/j.apsusc.2015.09.111.

[30] Y. Zhao, C.A. Wang, Nano-network MnO2/polyaniline composites with enhanced electrochemical properties for supercapacitors, Mater. Des. 97 (2016) 512–518, https://doi.org/10.1016/j.matdes.2016.02.120.

[31] L. Ma, X. Shen, Z. Ji, G. Zhu, H. Zhou, Ag nanoparticles decorated MnO2/reduced graphene oxide as advanced electrode materials for supercapacitors, Chem. Eng. J. 252 (2014) 95–103, https://doi.org/10.1016/j.cej.2014.04.093.

[32] F. Cheng, Y. Su, J. Liang, Z. Tao, J. Chen, MnO2-based nanostructures as catalysts for electrochemical oxygen reduction in alkaline media, Chem. Mater. 22 (2010) 898–905, https://doi.org/10.1021/cm901698s.

[33] Y.L. Chan, S.Y. Pung, S. Sreekantan, F.Y. Yeoh, Photocatalytic activity of β-MnO2 nanotubes grown on PET fibre under visible light irradiation, J. Exp. Nanosci. 11 (2016) 603–618, https://doi.org/10.1080/17458080.2015.1102342.

[34] A. Iyer, H. Galindo, S. Sithambaram, C. King'ondu, C.H. Chen, S.L. Suib, Nanoscale manganese oxide octahedral molecular sieves (OMS-2) as efficient photocatalysts in 2-propanol oxidation, Appl. Catal. A Gen. 375 (2010) 295–302, https://doi.org/10.1016/j.apcata.2010.01.012.

[35] M. Sharma, D. Choudhury, S. Hazra, S. Basu, Effective removal of metal ions from aqueous solution by mesoporous MnO2 and TiO2 monoliths: kinetic and equilibrium modelling, J. Alloy. Comp. 720 (2017) 221–229, https://doi.org/10.1016/j.jallcom.2017.05.260.

[36] M. Gheju, I. Balcu, G. Mosoarca, Removal of Cr(VI) from aqueous solutions by adsorption on MnO2, J. Hazard Mater. 310 (2016) 270–277, https://doi.org/10.1016/j.jhazmat.2016.02.042.

[37] S.T. El-Wakeel, R.S. El-Tawil, H.A.M. Abuzeid, A.E. Abdel-Ghany, A.M. Hashem, Synthesis and structural properties of MnO2 as adsorbent for the removal of lead (Pb2+) from aqueous solution, J. Taiwan Inst. Chem. Eng. 72 (2017) 95–103, https://doi.org/10.1016/j.jtice.2017.01.008.

[38] M.X. Zhu, Z. Wang, S.H. Xu, T. Li, Decolorization of methylene blue by δ-MnO2-coated montmorillonite complexes: emphasizing redox reactivity of Mn-oxide coatings, J. Hazard Mater. 181 (2010) 57–64, https://doi.org/10.1016/j.jhazmat.2010.04.080.

[39] Y. He, D. Bin Jiang, J. Chen, D.Y. Jiang, Y.X. Zhang, Synthesis of MnO2 nanosheets on montmorillonite for oxidative degradation and adsorption of methylene blue, J. Colloid Interface Sci. 510 (2018) 207–220, https://doi.org/10.1016/j.jcis.2017.09.066.

[40] A. Gagrani, J. Zhou, T. Tsuzuki, Solvent free mechanochemical synthesis of MnO2for the efficient degradation of Rhodamine-B, Ceram. Int. 44 (2018) 4694–4698, https://doi.org/10.1016/j.ceramint.2017.12.050.

[41] B. Gnana Sundara Raj, A.M. Asiri, A.H. Qusti, J.J. Wu, S. Anandan, Sonochemically synthesized MnO2 nanoparticles as electrode material for supercapacitors, Ultrason. Sonochem. 21 (2014) 1933–1938, https://doi.org/10.1016/j.ultsonch.2013.11.018.

[42] N. Kaur, R.A. Mir, O.P. Pandey, Electrochemical and optical studies of facile synthesized molybdenum disulphide (MoS2) nano structures, J. Alloy. Comp. 782 (2019) 119–131, https://doi.org/10.1016/j.jallcom.2018.12.145.

[43] C. Wan, L. Yuan, H. Shen, Effects of electrode mass-loading on the electrochemical properties of porous MnO2 for electrochemical supercapacitor, Int. J. Electrochem. Sci. 9 (2014) 4024–4038.
[44] S. Devaraj, N. Munichandraiah, Effect of crystallographic structure of MnO2 on its electrochemical capacitance properties, J. Phys. Chem. C 112 (2008) 4406–4417, https://doi.org/10.1021/jp7108785.
[45] S.A. Alzahrani, S.A. Al-Thabaiti, W.S. Al-Arjan, M.A. Malik, Z. Khan, Preparation of ultra long α-MnO2 and Ag@MnO2 nanoparticles by seedless approach and their photocatalytic performance, J. Mol. Struct. 1137 (2017) 495–505, https://doi.org/10.1016/j.molstruc.2017.02.068.
[46] K.S. Prasad, A. Patra, Green synthesis of MnO2 nanorods using Phyllanthus amarus plant extract and their fluorescence studies, Green Process. Synth. 6 (2017) 549–554, https://doi.org/10.1515/gps-2016-0166.
[47] X. Zhang, M. He, P. He, C. Li, H. Liu, X. Zhang, Y. Ma, Ultrafine nano-network structured bacterial cellulose as reductant and bridging ligands to fabricate ultra-thin K-birnessite type MnO2 nanosheets for supercapacitors, Appl. Surf. Sci. 433 (2018) 419–427, https://doi.org/10.1016/j.apsusc.2017.10.053.
[48] S. Saha, A. Pal, Microporous assembly of MnO2 nanosheets for malachite green degradation, Separ. Purif. Technol. 134 (2014) 26–36, https://doi.org/10.1016/j.seppur.2014.07.021.
[49] B. Liu, I.M. Mosa, W. Song, H. Zheng, C.-H. Kuo, J.F. Rusling, S.L. Suib, J. He, Unconventional structural and morphological transitions of nanosheets, nanoflakes and nanorods of AuNP@MnO2, J. Mater. Chem. A. 4 (2016) 6447–6455, https://doi.org/10.1039/C6TA02017H.
[50] W. Tang, X. Wu, D. Li, Z. Wang, G. LIu, H. Liu, Y. Chen, Oxalate route for promoting activity of manganese oxide catalysts in total VOCs' oxidation : effect of calcination temperature and preparation method, J. Mater. Chem. A. 2 (2014) 2544–2554, https://doi.org/10.1039/c3ta13847j.
[51] J. Diaz-Angulo, I. Gomez-Bonilla, C. Jimenez-Tohapanta, M. Mueses, M. Pinzon, F. Machuca-Martinez, Visible-light activation of TiO2 by dye-sensitization for degradation of pharmaceutical compounds, Photochem. Photobiol. Sci. (2019), https://doi.org/10.1039/C8PP00270C.
[52] P. Wilhelm, D. Stephan, Photodegradation of rhodamine B in aqueous solution via SiO2@TiO2 nano-spheres, J. Photochem. Photobiol. A Chem. 185 (2007) 19–25, https://doi.org/10.1016/j.jphotochem.2006.05.003.
[53] R.A. Mir, O.P. Pandey, Influence of graphitic/amorphous coated carbon on HER activity of low temperature synthesized β-Mo2C@C nanocomposites, Chem. Eng. J. 348 (2018) 1037–1048 https://doi.org/10.1016/j.cej.2018.05.041.
[54] L.K. Brar, A. Gupta, O.P. Pandey, Influence of carbon content of nano-TaC powders on the electrocatalytic and photocatalytic properties, Catal. Today 325 (2018) 98–108, https://doi.org/10.1016/j.cattod.2018.07.053.
[55] S.K. Meher, G.R. Rao, Enhanced activity of microwave synthesized hierarchical MnO2 for high performance supercapacitor applications, J. Power Sources 215 (2012) 317–328, https://doi.org/10.1016/j.jpowsour.2012.04.104.
[56] Y. Zhang, C. Sun, P. Lu, K. Li, S. Song, D. Xue, Crystallization design of MnO2 towards better supercapacitance, CrystEngComm 14 (2012) 5892–5897, https://doi.org/10.1039/c2ce25610j.
[57] B. Zhao, M. Lu, Z. Wang, Z. Jiao, P. Hu, Q. Gao, Y. Jiang, L. Cheng, Self-assembly of ultrathin MnO2/graphene with three-dimension hierarchical structure by ultrasonic-assisted co-precipitation method, J. Alloy. Comp. 663 (2016) 180–186, https://doi.org/10.1016/j.jallcom.2015.12.018.
[58] X. Zhao, Y. Hou, Y. Wang, L. Yang, L. Zhu, R. Cao, Z. Sha, Prepared MnO2 with different crystal forms as electrode materials for supercapacitors: experimental research from hydrothermal crystallization process to electrochemical performances, RSC Adv. 7 (2017) 40286–40294, https://doi.org/10.1039/c7ra06369e.
[59] M.R. Lukatskaya, B. Dunn, Y. Gogotsi, Multidimensional materials and device architectures for future hybrid energy storage, Nat. Commun. 7 (2016), https://doi.org/10.1038/ncomms12647.
[60] M.-K. Song, S. Cheng, H. CHen, W. Qin, K.-W. Nam, S. Xu, Z.-Q. Yang, A. Bongiorno, J. Lee, J. Bai, T.A. Tyson, J. Cho, M. Liu, Anomalous pseudocapacitive behavior of a nanostructured, mixed- valent manganese oxide film for electrical energy storage, Nano Lett. 12 (2018) 3483–3490, https://doi.org/10.1021/nl300984y.